Winglets on Low-Aspect-Ratio Wings

John M. Kuhlman* and Paul Liaw†
West Virginia University, Morgantown, West Virginia

A preliminary numerical design study has been conducted to assess the drag reduction potential of winglets installed on a series of low-aspect-ratio wings at a high subsonic Mach number cruise design point of $M=0.8$, $C_L \cong 0.3$. Wing/winglet and wing-alone design geometries have been obtained for wings of aspect ratios between 1.75 and 2.67, having a taper ratio of 0.2, and leading-edge sweep angles of 45–60 deg. Winglet length has been fixed at 15% of the wing semispan. To assess the relative performance between wing/winglet and wing-alone configurations at the selected design point, the PPW nonlinear extended small-disturbance potential flow analysis code has been utilized. Predicted decreases in pressure drag coefficients for the wing/winglet configurations relative to the corresponding wing-alone planforms are about 15% at the design point of $M=0.8$, $C_L \cong 0.3$. Predicted decreases in wing/winglet total drag coefficients are about 12% relative to the corresponding wing-alone design. These predicted percentage drag coefficient reductions are comparable to reductions already demonstrated by actual winglet designs installed on higher-aspect-ratio transport-type aircraft. Since the low-aspect-ration configurations have much lower lift-to-drag ratios, the overall drag force reduction for a low-aspect-ratio wing should be significantly larger than at higher aspect ratios. Also, the wing/winglet designs may be advantageous for supersonic flight, relative to a higher-aspect-ratio wing, since the winglet can be oriented to remain behind the Mach cone and because the wing/winglet wing designs have less twist than the wing-alone configurations.

Introduction

THE winglet concept originally developed by Whitcomb[1] has proved to be an effective means of reducing aircraft-induced drag through use of a nonplanar lifting system. The wing-tip-mounted, nearly vertical winglet develops a normal force that alters the configuration span load to diffuse the total circulation in the rolled-up wing tip vortex and reduce the total energy of the vortex.[2] Also, toe-out of the winglet allows the winglet normal force to develop a thrust component to reduce drag. Asai[3] has also shown the importance of the relatively short chord of the winglet to minimize the increased wetted area and resulting skin-friction penalty.

The winglet concept has to date primarily been applied to relatively high-aspect-ratio transport-type configurations (e.g., Refs. 1, 2, and 4). However, an early numerical study by Cary[5] indicated that larger reductions in induced drag force were obtainable at fixed lift for a given winglet as the aspect ratio of the wing on which it was installed was reduced. Another theoretical parametric study by Heyson et al.[6] found that winglet benefits, relative to a wing tip extension, increased as the wing aspect ratio decreased for a series of straight and swept, tapered and untapered wings. These early numerical results indicate that there should be a greater potential for induced drag force reduction and improvements in the cruise performance for the low-aspect-ratio, high-sweep wings typical of fighter aircraft than for the transport-type wings that have been emphasized previously. The present work has been undertaken based on the premise that the drag reduction capability of winglets already proved at high aspect ratios should logically carry over to winglets designed for wings of lower aspect ratio.

One existing wing/winglet design for a relatively low-aspect-ratio wing is that of the HiMAT research aircraft.[7] This configuration has an aspect ratio 3.85 wing fitted with wing tip fins, or winglets, that are 23% of the wing semispan in length. Winglet root chord is equal to wing tip chord. These winglets were found to reduce induced drag, but not by the amount predicted by linear theory. Also, performance was degraded at high-lift, transonic maneuver conditions, apparently due to extensive flow separation on the winglets. This is at least partially the result of the linear design methods that were utilized in the winglet design.[7] More recent nonlinear analyses[8] using the PPW code[9-11] for the HiMAT configuration have matched actual flight test data quite well. Also, Hackett[12] has recently presented results of a preliminary low-speed experimental study wherein a simple, untwisted, vertical vane was used to reduce drag of a low-aspect-ratio delta wing under separated flow conditions. Thus, there appear to be very few previous instances where winglets have been utilized on low-aspect-ratio wings.

The present effort is a preliminary design study to further assess the potential for winglets to reduce drag of low-aspect-ratio, high-sweep fighter-type wings at a high subsonic Mach number. The nonlinear transonic potential flow analysis code PPW[9-11] has been utilized to predict transonic performance for several wing/winglet and wing-alone planforms at a Mach number of 0.8 and lift coefficient of 0.3. Initial wing/winglet and wing-alone design geometries have been generated for attached flow using two existing linearized theory aerodynamic design codes[13-16] and wing/winglet geometries have then been altered as required in the wing/winglet juncture region.

Design Approach

General Philosophy

The present work has been conducted as an initial step to better determine the potential for winglets to reduce the drag of low-aspect-ratio fighter-type wings at a high subsonic Mach number. The basic philosophy of the work has been to use as simple a set of configuration geometries and analysis tools as are practical to still allow meaningful conclusions to be drawn.

At the simplest level, consider the induced drag efficiency factor k, defined as the ratio of induced drag coefficient for an

Received June 23, 1987; presented as Paper 87-2482CP at the AIAA 5th Applied Aerodynamics Conference, Monterey, CA, Aug. 17–19, 1987; revision received May 12, 1988.

*Professor, Department of Mechanical and Aerospace Engineering. Senior Member AIAA.

†Graduate Research Assistant, Department of Mechanical and Aerospace Engineering.

elliptically loaded planar wing to the induced drag coefficient of the optimal nonplanar wing/winglet configuration having an equal projected span at equal lift coefficient. The induced drag efficiency may be calculated using a Trefftz plane model, as shown in Fig. 1. These results have been taken from Refs. 13 and 17 and are identical to results of another numerical model by Lundry and Lissaman.[18] For vertical winglets, the Trefftz plane model predicts the efficiency factor increases linearly with winglet height ℓ. To a good approximation, k-1 is equal to the ratio of winglet length to semispan. Thus, for typical winglet lengths of 10–20% of the wing semispan, the potential percentage reduction in induced drag coefficient $1-1/k$ is 9–17%. In Fig. 1, k has been calculated assuming that the nonplanar configuration has the same projected span as the planar wing; hence, the nonplanar configuration will have a longer actual length. For results of the present study, comparisons between wing-alone and wing/winglet performance have instead been made by holding the wing area fixed and allowing the wing/winglet projected span to increase slightly (3.9%). The Trefftz plane model predicts k to be independent of both C_L and wing aspect ratio.

Assuming then that wing/winglet geometries could be designed to develop the required spanload independent of wing-aspect ratio, the following simple argument will indicate why a winglet should have a larger impact for a low-aspect-ratio wing. The optimum induced drag coefficient, including nonplanar effects, is given by

$$C_{Di} = C_L^2/(\pi A k) \tag{1}$$

Thus, ignoring the dependence of lift curve slope on A and holding C_L fixed, it is seen that C_{Di} will vary inversely with Ak. Applying the far-field results of Fig. 1, where k is predicted to be independent of wing-aspect ratio, it is seen that the percent reduction in induced drag coefficient for a fixed value of $\ell/(b/2)$ should not vary with wing-aspect ratio. This leads to the conclusion that the actual reduction in induced drag force at fixed lift would be significantly larger for a winglet installed on a low-aspect-ratio wing, since the lift-to-drag ratio would be smaller.

Equation (1) may also be written in dimensional form as

$$D_i = (L/b)^2/(\pi q k) \tag{2}$$

where q is dynamic pressure. Thus, it is seen that the induced drag is dependent on the square of the ratio of lift to span. This equation may be interpreted as indicating that the induced drag is independent of aspect ratio. However, additional structural considerations would indicate that a lower-aspect-ratio wing of equal structural weight could safely develop a higher wing loading than a high-aspect-ratio wing. Even ignoring this structural advantage and simply requiring a constant wing loading, it is seen that, for a given configuration weight, as aspect ratio is decreased the span must decrease, thereby increasing induced drag by the span ratio squared at fixed lift [Eq. (2)].

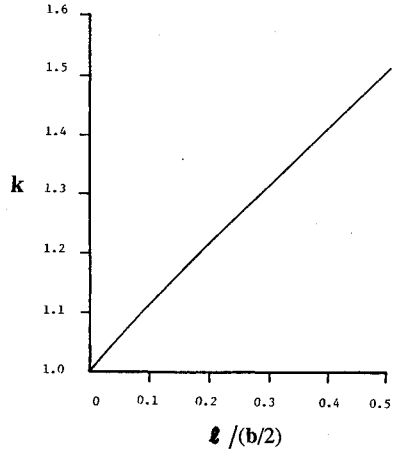

Fig. 1 Predicted performance benefits of winglets based on far-field theory.[13,17]

It should be noted that the potential drag reductions predicted using far-field theory are expected to be optimistic, especially at high lift, since no additional drag penalties are included for the added wetted area or added wave drag due to any shocks on the winglets or adverse mutual interference between wing and winglet. However, this application of a simple far-field minimum induced drag calculation highlights the very significant potential of properly designed winglets to reduce drag. In particular, the potential percentage reduction in total configuration drag coefficient at high lift coefficients approaches the percentage reduction in induced drag coefficient, which is directly proportional to winglet length (Fig. 1).

Planform Choices

Choices of both wing and winglet planform in the present study have been influenced by four basic considerations. First, an effort has been made to study a range of wing/winglet planforms that might be representative of typical wing aspect ratio and leading-edge sweep values for present[19–21] and next-generation[22–25] fighter aircraft. Second, concerns over the ability of the linear design methodology utilized to generate wing/winglet geometries that developed realistic enough wing and winglet loadings to permit converged, essentially attached flow solutions to be obtained from the PPW code at the selected high subsonic Mach number cruise design point also influenced the range of wing and winglet planforms selected. Third, difficulties encountered in obtaining converged transonic flow solutions[21] with an early version of the PPW code for a wing of aspect ratio 3 influenced early wing planform choices. It has since been learned that this early problem has been alleviated by implementation of a different crude grid developed by Waggoner.[26] Related to this issue, limitations of the PPW code have influenced the range of winglet geometries studied. Fourth, it has also been possible to investigate trends in predicted drag reduction vs wing aspect ratio or sweep.

Based on these considerations, an initial series of design studies have focused on the series of eight trapezoidal wing planforms defined in Table 1. These wings have aspect ratios of 1.75–2.67, leading-edge sweep angles of 45–60 deg, and a constant value of taper ratio of 0.2. Note that Φ in Table 1 is the wing trailing-edge sweep angle. These wing planform values were believed to bracket current and next-generation fighter configurations[19–25] and to include high enough values of the aspect ratio to ensure that at least some successfully converged transonic flow solutions would be obtained.

For this initial study, a trapezoidal winglet planform was selected for each wing, where winglet length, cant, taper ratio, and leading-edge sweep were the same for all configurations. Winglet trailing-edge sweep was varied as required to maintain a constant ratio of winglet area to wing area. Winglet length was fixed at 15% of the wing semispan, so that the far-field drag analysis predicts each configuration should have the potential to achieve nominally a 13% reduction in induced drag when configuration projected span is held fixed or 16.9% when wing area is held fixed. Winglet leading-edge sweep was fixed at 50 deg; wing leading-edge sweep angles bracket this

Table 1 Wing planform configurations

Configuration	A	Λ, deg	Φ, deg	λ
A	2.63	50	10	0.2
B	2.67	45	0	0.2
C	1.75	50	−18.4	0.2
D	1.75	55	− 5.5	0.2
E	1.75	60	11.8	0.2
F	2.20	45	−12.0	0.2
G	2.20	50	− 1.2	0.2
H	2.20	55	12.2	0.2

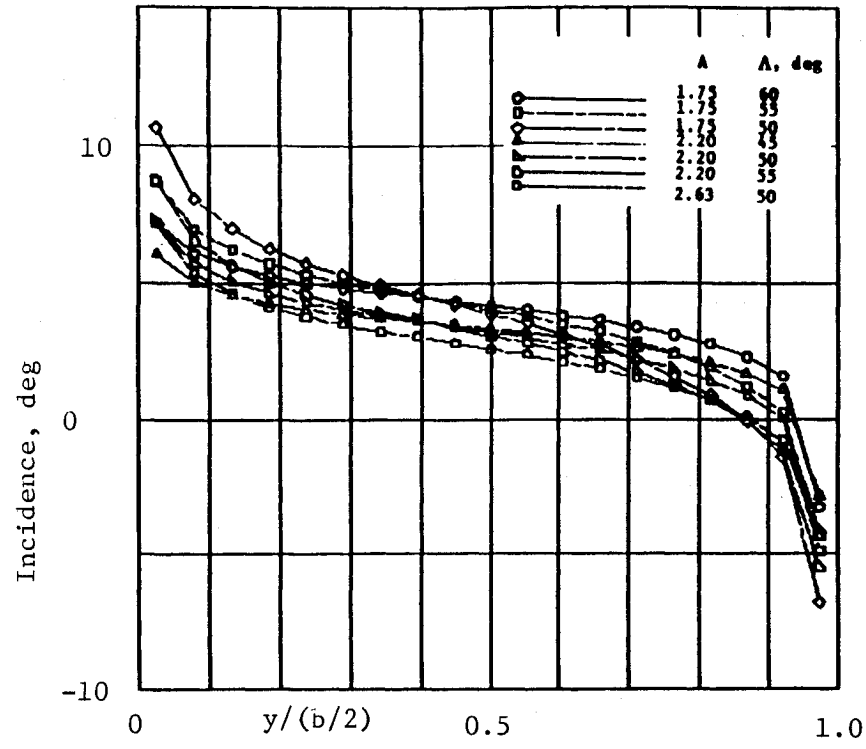

Fig. 2 Incidence distributions for linear theory minimum induced drag designs at $M = 0.8$, $C_L \cong 0.3$ for wing-alone configurations of Table 1.

value. All winglets so defined have total areas equal to 2.25% of the basic wing area. These chosen winglet length and area values are consistent with those used in previous winglet applications.[1,3,4,7,19] Other winglet planform details have been selected primarily based upon Whitcomb's original recommendations,[1] aimed at reducing adverse mutual interference effects. Thus, winglets have been located in an aft position, behind the wing tip airfoil shoulder. Since all wing and winglet configurations have utilized an NACA 64A006 thickness distribution, winglet root chord was fixed at 60% of the wing tip chord. Cant was fixed at 15 deg and has not been varied in the present study because the version of PPW used utilizes a rectangular intermediate grid and a vertical winglet computational orientation. Winglet taper ratio has been fixed at 0.5 in the current work due to concerns about inadequate grid resolution in the PPW code for smaller winglet tip chords. Further discussion of the design approach may be found in Ref. 27.

Design Point

Actual fighter aircraft designs are the result of tradeoffs between a number of competing design points or mission requirements, [28] which have not been addressed in the present study. Instead, for the present work, a cruise condition at a high subsonic Mach number has been selected for all designs, based on the belief that existing fighter aircraft typically cruise at as high a Mach number as possible without a significant drag rise penalty (i.e., $0.7 \leq M \leq 0.9$ at cruise). Thus, a single value of $M = 0.8$ has been selected as the design Mach number value. Also, based on typical and maximum wing loadings and wing areas for existing lightweight fighters,[19] typical configuration lift coefficients at $M = 0.8$ at an altitude of 30,000 ft range from about 0.2 for a lightly loaded, "clean" configuration to about 0.4 for a very heavily loaded configuration. Thus, a single design value of lift coefficient of $C_L \cong 0.3$ has been selected for the present study since it falls in the appropriate range, but is also high enough so that a significant potential for total drag reduction exists (an order of magnitude of 10% including the fuselage, estimated from Fig. 1).

Design Methodology

An overview of the numerical design process and design tools utilized in the present work will now be given. First, for each configuration of interest, the wing planform, design point, and winglet orientation and planform are fixed as described above. Then, either of two aerodynamic design codes are utilized to generate initial linearized attached flow theory wing and winglet geometry input for the more sophisticated nonlinear transonic analysis code of Refs. 9–11. Also, cylindrical fuselage definition is added at this point, where fuselage diameter is 25% of the wing semispan. Fuselage length is 10.5 times the wing semispan, to approximate an infinite cylinder. The PPW analysis code is then utilized to analyze configuration performance at the transonic design point. The original linear theory winglet design geometry is also modified to improve the configuration performance as predicted by the PPW analysis code. In particular, wing tip and winglet incidence values have been altered to weaken shocks predicted by the nonlinear analysis code to reduce wave drag.

Both linear design programs[13–16] have been modified to generate output files of linear theory optimum wing and winglet upper and lower surface coordinates in the format required for the PPW nonlinear analysis code. A second file in Hess format is also generated for interactive plotting of the resulting geometry.[29]

The PPW nonlinear transonic analysis code[9–11] solves a finite-difference representation of an extended small-disturbance form of the nonlinear full potential equation by a relaxation method. The extensions to the classical transonic small-disturbance equation are nonlinear terms that appear in the full potential equation, which improve the ability to capture swept shocks on the wing and winglet.

A unique feature of the code is the utilization of multiple, nested, rectangular grids with fine resolution in regions of large flow gradients. Variation in flowfield potential is communicated from one grid system to another by interpolation. Use of these multiple grids allows good resolution of the flowfield details around a winglet without requiring a very fine grid away from the winglet. In addition, no complex grid generation is required, so that configuration components can very easily be added or removed to study interference effect trends.

The small-disturbance formulation has also been used to simplify boundary conditions, which are applied at the nearest neighboring computational grid points. Boundary conditions are corrected by small-disturbance theory for variation due to

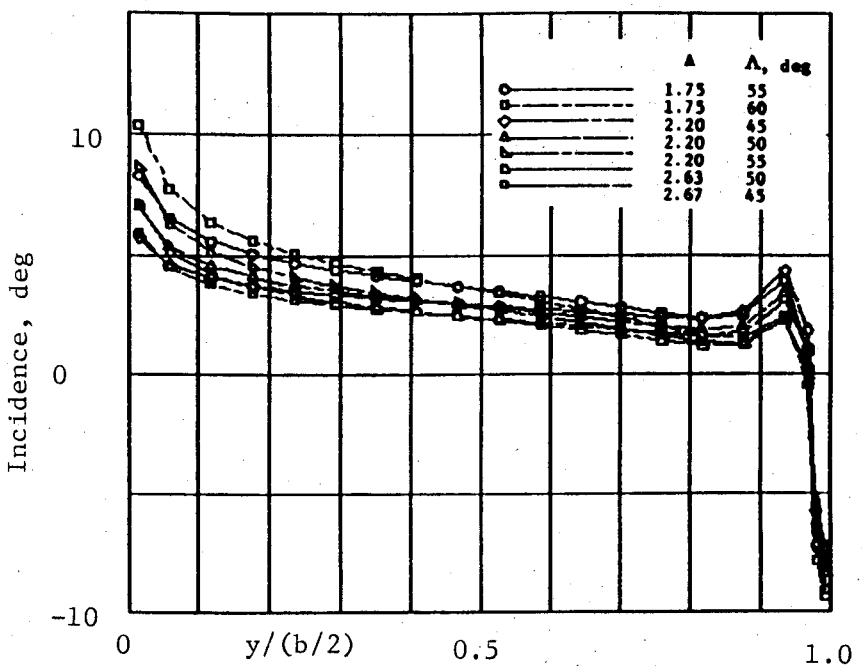

Fig. 3 Incidence distributions for linear theory minimum induced drag designs at $M = 0.8$, $C_L \cong 0.3$ for wing configurations of Table 1 fitted with $0.15(b/2)$ winglets.

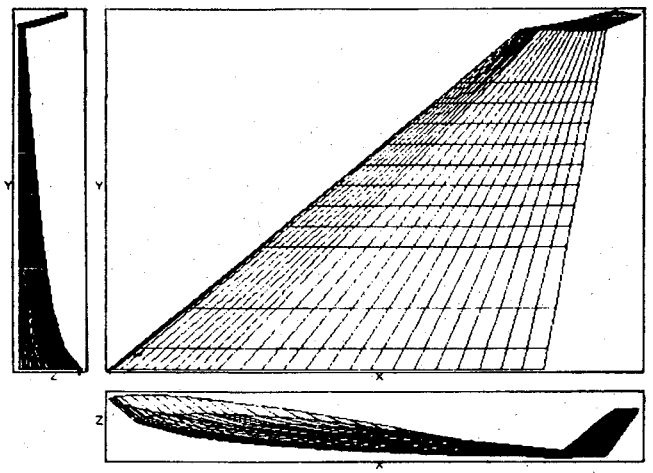

a) Wing A ($A = 2.63$, $\Lambda = 50$ deg, $\lambda = 0.2$)

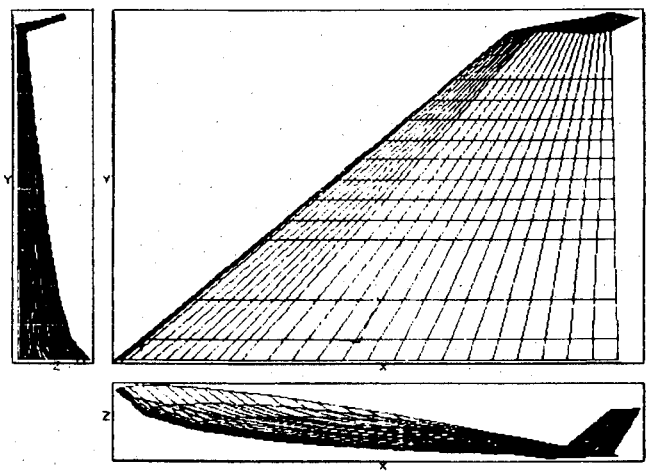

b) Wing G ($A = 2.20$, $\Lambda = 50$ deg, $\lambda = 0.2$)

Fig. 4 Wing-winglet geometry for $M = 0.8$, $C_L \cong 0.3$; $0.15(b/2)$ winglets.

differences in location of the physical boundary and the computational boundary.

A two-dimensional, compressible strip boundary-layer calculation may be performed on the wing surfaces using simple sweep theory and interacted with the outer potential flow. The boundary-layer displacement thickness is calculated and used to modify the wing surface slope boundary conditions. Configuration forces and moments and spanload distributions are calculated by direct numerical integration of the pressure coefficient distributions. No boundary-layer calculations are performed on the fuselage, winglet, pods, or pylons. Viscous effects are estimated for the fuselage and winglet using a flat-plate skin-friction correlation corrected for compressibility effects.

Results

Results of the present study will be presented by first describing the linear theory design geometries and required modifications to these geometries to obtain successfully converged nonlinear transonic flow results at the chosen design point. Then, the transonic flow results will be presented; convergence will be discussed first, followed by comparison of the predicted performance levels.

Linear Theory Designs

All results to be presented in the present paper have used the first design code[13,14] to define minimum induced drag wing-alone and wing/winglet camber surfaces for each of the eight wing planforms listed in Table 1. Seven of the resulting incidence distributions for the optimum wing-alone geometries are shown in Fig. 2, while similar incidence plots for the wing/winglet configurations are shown in Fig. 3. Optimum wing incidence is characterized by a gradual washout, except in the vicinity of the wing root and wing tip where much more rapid washout is observed. In contrast, wing/winglet incidence follows the wing-alone distribution inboard, but shows a dramatic increase in wing tip incidence, while most of the winglet is toed out (negative incidence in Fig. 3). Also note that the winglet root airfoil is toed in somewhat. This is accompanied by a rather large amount of camber. These unexpected kinks in wing tip and winglet root incidence have been found not to be a result of any poor paneling choices in the linear theory design code. Examples of the resulting wing/winglet geometries for two of the $\Lambda = 50$ deg wings are shown in Fig. 4.

PPW Analysis Code Convergence Results

As an initial step in utilizing the PPW nonlinear transonic code to analyze performance of low-aspect-ratio wing/winglet

configurations, the convergence capabilities of this program were studied for the eight trapezoidal wing planforms described in Table 1. This was done partially because of concern over convergence difficulties encountered previously by others at low aspect ratio.[21] A second purpose of this study was to establish the viability of using the simple linear theory design methods described above to define the initial low-aspect-ratio wing-alone and wing/winglet design geometries.

All eight of the wing-alone configurations designed by the linear theory design code were found to yield successfully converged, realistic flowfield solutions at $M=0.8$, $\alpha=0.5$ deg using the PPW code, without alteration of the geometry, when no interaction of the viscous boundary layer was used for 160 iterations (100 crude grid, followed by 60 crude-fine grid iterations). Here, the term "realistic" is used to indicate a PPW solution without significant oscillations in the surface pressure coefficient distributions. Angle of attack has been increased by 0.5 deg because this has often been found to provide better agreement with experiment.[11] Maximum changes in the flowfield potential ranged from 1.7×10^{-5} to 6.5×10^{-5}. When wing viscous boundary-layer interaction was included, convergence difficulties were observed at the lowest aspect ratio for the higher wing sweep angles. Wing E ($A=1.75$, $\Lambda=60$ deg) would not converge, while the PPW solution for wing D ($A=1.75$, $\Lambda=55$ deg) at $\alpha=0.5$ deg also diverged, but converged at $\alpha=0$ deg. Maximum changes in solution potential with the interacted boundary layer using 300 iterations (100 crude grid and 200 crude-fine grid iterations) ranged from 5.7×10^{-6} and 6.6×10^{-5} for the seven wing-alone configurations. Thus, it has been found that converged, realistic transonic flowfield solutions may be obtained from the PPW code at $M=0.8$, $C_L\cong0.3$ for a series of trapezoidal low-aspect-ratio wings of $1.75\leq A\leq2.67$, $45\leq\Lambda\leq55$ deg, with $\lambda=0.2$, where wing camber and twist have been defined by linear theory.

However, much greater difficulty was encountered in obtaining realistic, converged nonlinear PPW solutions for the eight wing/winglet configurations. No converged solutions were obtained for any of these geometries when used exactly as specified by the linear design code. However, converged, realistic solutions were obtained for all but two wing/winglet configurations when the original geometries were modified to reduce loading at the wing tip and winglet root, by omitting the wingtip incidence kink and the highly swept, highly cambered, toed in winglet root airfoils. Instead, the wing tip and winglet root airfoils were defined using the airfoils inboard on the wing or upward on the winglet. The levels of convergence for the higher- and intermediate-aspect-ratio wing/winglet configurations were comparable to those observed for the corresponding wing-alone configuration. Even greater difficulty was experienced in obtaining converged PPW solutions for the $A=1.75$ wing/winglet configurations than for the wing-alone cases. This is believed to most likely be due to inadequacy of the linear design methodology at the lower aspect ratios rather than to any inherent limitation to the PPW code itself.

PPW Analysis Code Performance Comparisons

The potential for winglets to reduce drag for low-aspect-ratio wings at a transonic cruise design point has been assessed by comparing the lift-to-drag ratios computed by the PPW code for each wing/winglet configuration with the calculated L/D for the corresponding optimum wing-alone configuration at essentially the same lift, as shown in Table 2. The percentage differences between calculated wing-alone and wing/winglet lift coefficients have also been shown. All lift and drag coefficients in this comparison have omitted the fuselage force

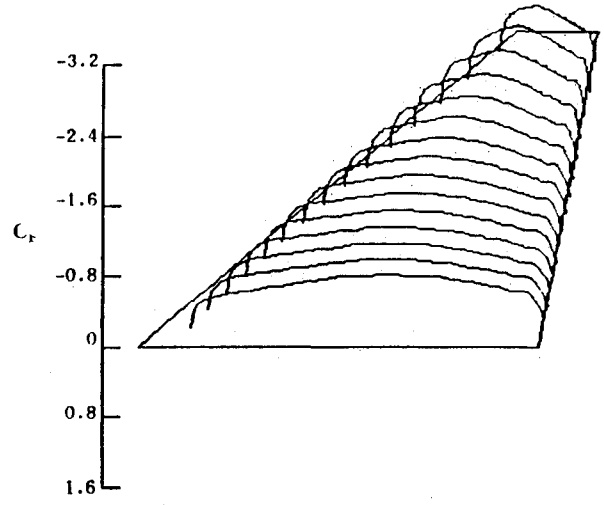

a) Wing A ($A=2.63$, $\Lambda=50$ deg, $\lambda=0.2$)

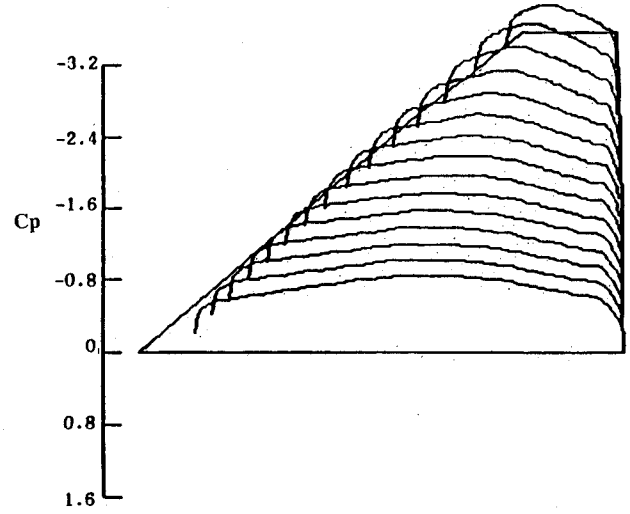

b) Wing G ($A=2.20$, $\Lambda=50$ deg, $\lambda=0.2$)

Fig. 5 Calculated upper surface pressure coefficient distributions for wing-alone designs at $M=0.8$, $\alpha=0.5$ deg, $C_L\cong0.3$ (160 iterations, no boundary layer).

Table 2 PPW code predicted lift-to-drag increases due to 0.15(b/2) winglets at $M=0.8$, $C_L\cong0.3$

Config.	Wing A	Wing λ, deg	160 iterations, no boundary layer C_L/C_{Dp} increase, %	ΔC_L, %	300 iterations, with boundary layer C_L/C_{Dp} incease, %	C_L/C_{Dtot} increase, %	ΔC_L, %
A	2.63	50	13.1	0.9	14.9	11.5	−0.8
B	2.67	45	14.4	−1.87	15.0	11.8	−1.2
D	1.75	55	16.4[a]				
				−0.02[a]	—	—	—
F	2.20	45	16.5	−0.99	15.8	13.3	−0.9
G	2.20	50	16.7	0.05	14.6	12.1	0.7
H	2.20	55	15.7	−1.23	—	—	—
C	1.75	50	14.9	−0.20	—	—	—

[a] $\alpha=0$ deg; all other cases at $\alpha=0.5$ deg.

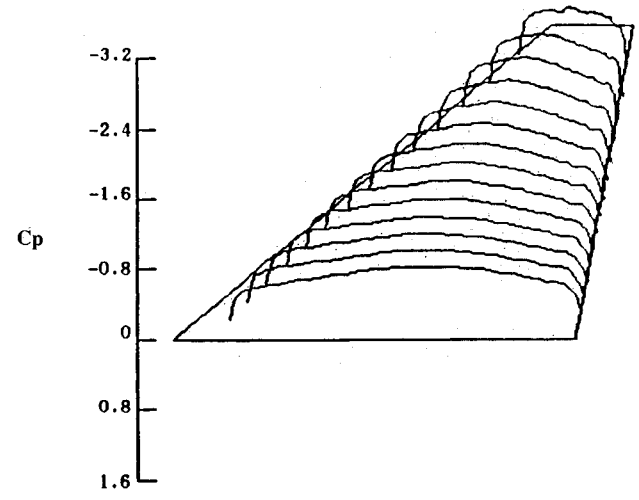

a) Wing A ($A = 2.63$, $\Lambda = 50$ deg, $\lambda = 0.2$)

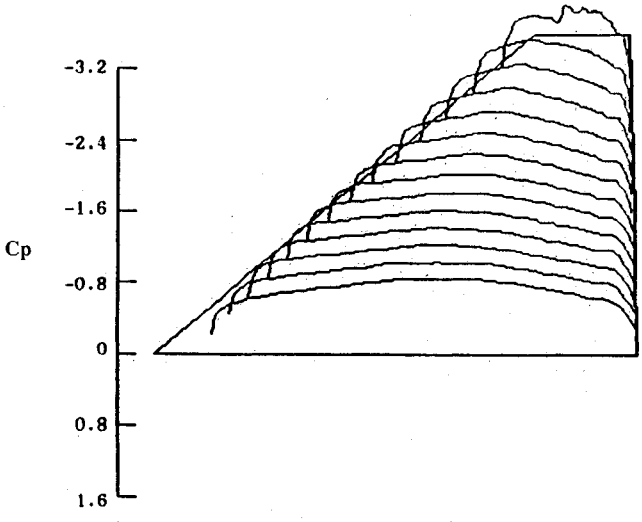

b) Wing G ($A = 2.20$, $\Lambda = 50$ deg, $\lambda = 0.2$)

Fig. 6 Calculated upper surface pressure coefficient distributions for wing of wing/winglet designs at $M = 0.8$, $\alpha = 0.5$ deg, $C_L \cong 0.3$ (160 iterations, no boundary layer).

coefficients, so comparisons have been made between the wing-plus-winglet force coefficients and the wing forces for the corresponding wing-alone configuration. All lift and drag force coefficients have been calculated using the configuration wing area as the reference area. Thus, force coefficient ratios are directly interpreted as ratios of forces. Lift coefficients have generally been matched to within approximately $\pm 1\%$.

Predicted increases in lift-to-pressure drag (induced drag plus wave drag) are between 13.1 and 16.7% for runs without boundary-layer interaction for 160 iterations. No clear trend in predicted percentage L/D increases is observed as the wing aspect ratio or leading-edge sweep angle is varied. When the wing/boundary-layer interaction is included and 300 iterations are used, calculated wing/winglet pressure drag is 14.6-15.7% lower than for the corresponding wing-alone configuration at essentially the same lift. For these four configurations, the calculated wing/winglet lift-to-total drag is 11.5–13.3% higher than calculated wing lift-to-total drag at the same lift. Again, there is no systematic variation of the predicted percentage L/D increases with wing aspect ratio or wing leading-edge sweep. Coding was added to use the calculated wing and winglet spanloads to calculate a bending moment coefficient about the wing root to allow some comparisons of the structural penalty due to the winglet. For the four configurations for which 300 iteration interacted boundary-layer solutions have been obtained, this calculated bending moment coeffi-

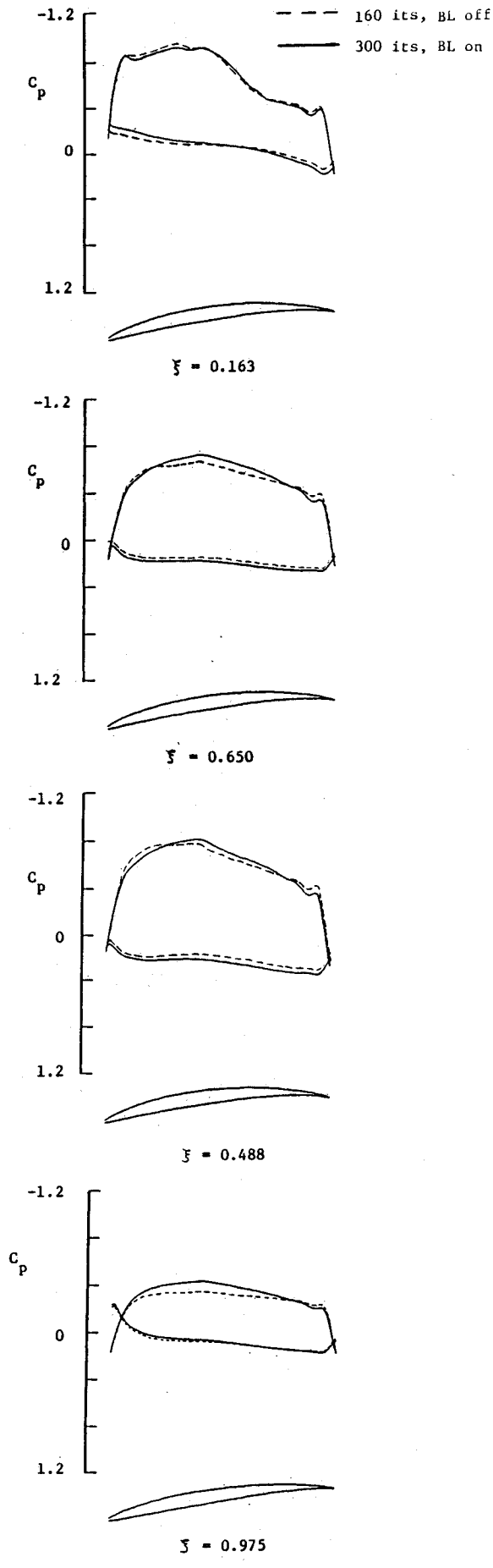

Fig. 7 Calculated winglet pressure coefficient distributions for wing A fitted with 0.15($b/2$) winglet at $M = 0.8$, $\alpha = 0.5$ deg, $C_L \cong 0.3$.

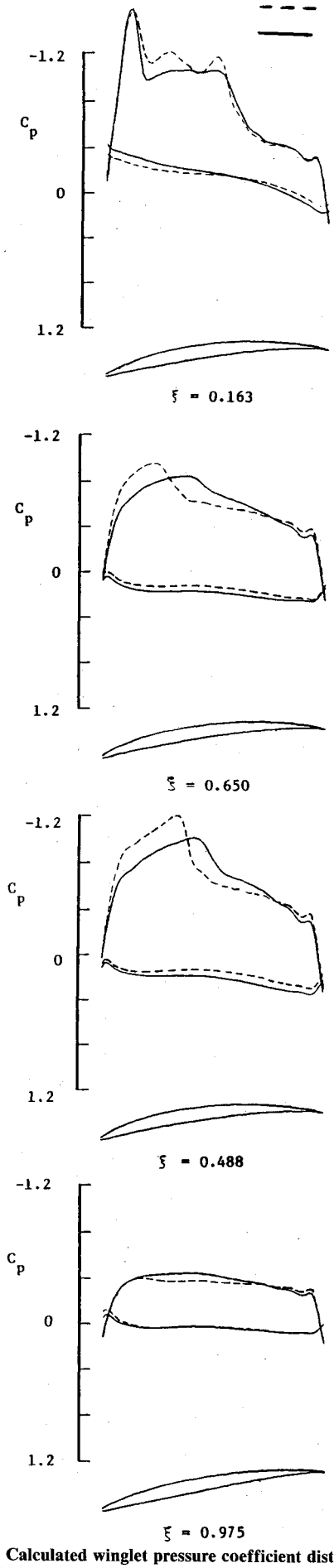

Fig. 8 Calculated winglet pressure coefficient distributions for wing G fitted with $0.15(b/2)$ winglet at $M=0.8$, $\alpha=0.5$ deg, $C_t \cong 0.3$.

cient at the design point was increased 5–7% for the wing/winglet case relative to the corresponding wing-alone case. These percentage increases in bending moment are of the same order as those calculated by Heyson et al.[6] for winglets on wings of similar aspect ratio.

Typical calculated upper surface wing-alone pressure coefficient distributions are shown in Fig. 5 for the $A=2.63$ and 2.20, $\Lambda=50$ deg configurations using 160 iterations without boundary-layer interaction. Results for the other wing-alone configurations all look quite similar. The corresponding wing upper surface pressure coefficient distributions for the $A=2.63$ and 2.20, $\Lambda=50$ deg wing/winglet configurations, again for 160 iterations and no boundary-layer interaction, are shown in Fig. 6. They are nearly identical to the wing-alone results except near the wing tip in the vicinity of the winglet. Here the presence of the winglet results in larger velocities and more negative pressure coefficient values. Examples of the calculated winglet pressure coefficients at $\xi=0.163$, 0.488, 0.650, and 0.975 (where ξ is the fractional distance from the winglet root to the winglet tip) are shown for the same two wing/winglet solutions in Figs. 7 and 8. Smooth, nearly rectangular winglet pressure distributions are obtained at $A=2.63$, but a shock is observed near midchord over the lower 50% of the

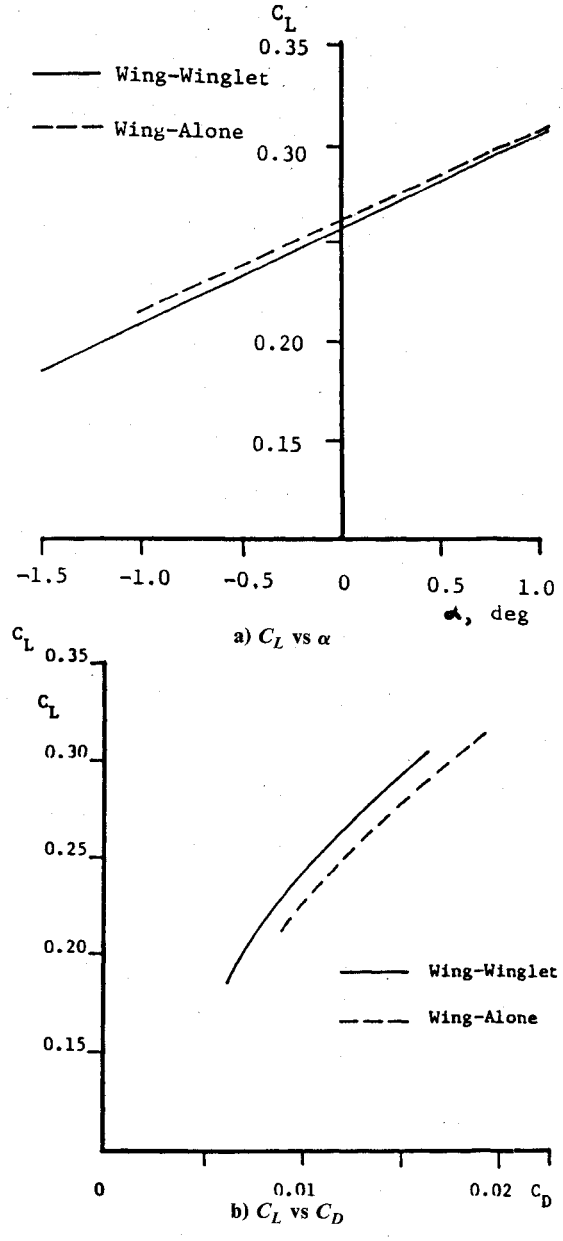

Fig. 9 Predicted performance of wing A fitted with $0.15(b/2)$ winglet at $M=0.8$ (300 iterations with boundary-layer interaction)

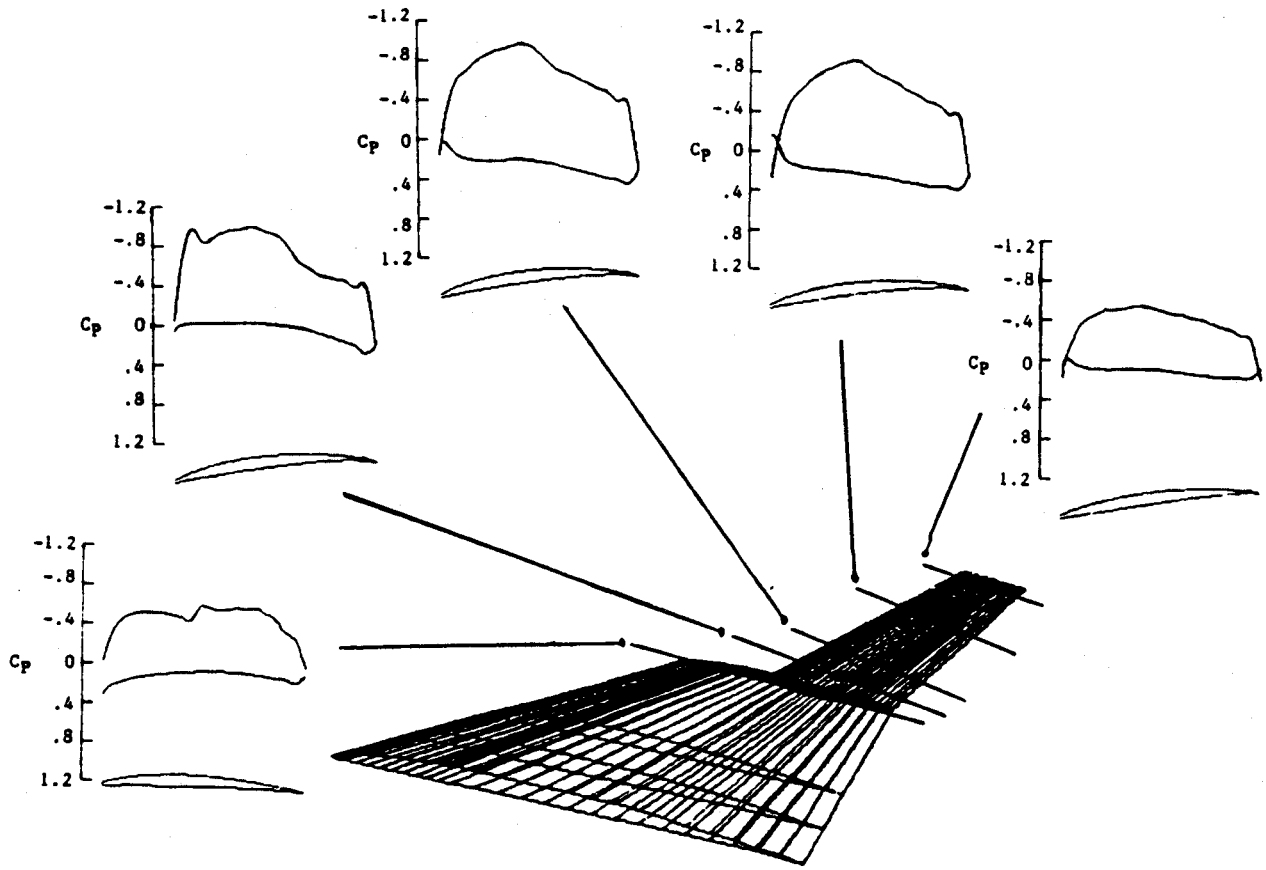

Fig. 10 Calculated pressure coefficient distributions for wing H ($A = 2.20$, $\Lambda = 55$ deg, $\lambda = 0.2$) fitted with $0.25(b/2)$, $\Lambda = 45$ deg winglet at $M = 0.8$, $\alpha = 0.5$ deg, $C_L \cong 0.3$ (300 iterations with boundary-layer interaction).

winglet at $A = 2.20$. In addition, a suction peak is observed at the winglet leading edge near the winglet root, indicating that this winglet should be toed out more. For the assumed $a = 1.0$ rectangular chord loading, there also appears to be a weak trailing-edge shock everywhere along the winglet ($C_p^* \cong -0.4$ at $M = 0.8$). Winglet pressure coefficients have been shown in Figs. 7 and 8 for both the 160 iteration, no boundary-layer solutions and the better-converged, more realistic solutions for 300 iterations with the interacted boundary layer. Very little difference is observed at $A = 2.63$. However, midchord shocks are weakened and moved slightly aft and trailing-edge shocks are weakened slightly for the solution including the interacted wing/boundary layer for the more heavily loaded winglet on the $A = 2.20$ wing. Similar trends have been seen for the effect of including the boundary layer on shock location for transport wing configurations in Ref. 26. Figure 9 shows the calculated performance at $M = 0.8$ vs angle of attack for case A. All results were obtained using 300 iterations and boundary-layer interaction. For $0.2 \leq C_L \leq 0.3$, the lift curve slope is constant. The wing/winglet drag polar appears to be shifted to lower drag.

Further examples of calculated pressure coefficient distributions obtained for a longer winglet of length equal to 0.25 $(b/2)$ on wing planform H ($A = 2.20$, $\Lambda = 55$ deg) are presented in Fig. 10. This configuration has a potential for a 25.4% reduction in induced drag coefficient relative to the shorter span wing-alone configuration, based on the far-field theory of Refs. 13 and 17. The winglet leading-edge sweep is 45 deg, taper ratio 0.5, and cant 15 deg. The design process and resulting geometry were both quite similar to those for the shorter 0.15 $(b/2)$ winglet configurations, with the exception that winglet twist had to be altered to obtain converged, smooth pressure coefficient solutions. This solution is at $M = 0.8$, $\alpha = 0.5$ deg for 300 iterations with the interacted boundary layer. For this run, the maximum change in flowfield potential was 3.43×10^{-5} and the wing/winglet lift coefficient is 0.2% low relative to the wing-alone results. The calculated lift-to-pressure drag ratio is increased 19.4% relative to the wing-alone case, while calculated wing/winglet lift-to-total drag ratio is increased 15.4% compared to the wing-alone case. Much smaller drag reductions at equal lift, of 14.9% in C_{Dp} and 11.9% in C_{Dtot} have been computed for a lower-sweep (30 deg), long winglet; this is due to the occurrence of strong shocks on the inboard winglet surface that results from a larger interference effect for the lower-sweep winglet.

Discussion

All of the present PPW nonlinear performance predicitions tend to support the much simpler trends discussed under design philosophy, using a far-field drag model. The predicted percentage drag coefficient reductions of the wing/winglet designs at fixed lift are largely independent of wing planform (aspect ratio and leading-edge sweep) and tend to scale directly proportional to the ratio of winglet length divided by wing semispan. Both of these trends are predicted by the simple far-field theory. Of course, these conclusions will remain valid only so long as smooth, attached flow is maintained on both the wing and winglet. Some limited efforts to obtain PPW solutions at higher lift coefficients for the configurations discussed in the present study have usually led to diverging, unstable solutions. In some general sense, this indicates that the actual flowfield would be too highly loaded on the winglet inboard surface or near the wing tip, so that shock-induced flow separation would be expected in these regions at higher lift coefficients. This could negate any drag reductions due to the winglet at high lift. However, it does appear possible to increase winglet toe out as C_L is increased, thereby maintaining attached flow over a wider range of lift coefficients. This leads one to the concept of an aeroelastically tailored or "steerable" winglet to maintain attached flow conditions over a range of lift coefficients.

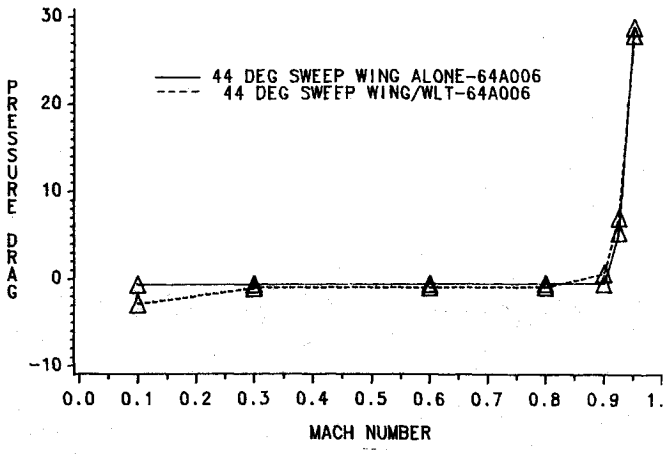

Fig. 11 Predicted pressure drag coefficient (in drag counts) at $C_L = 0$ for $A = 2.5$, $\lambda = 44$ deg, $\lambda = 0.2$ wing-alone and wing/winglet, without camber or twist (from Ref. 30).

While the present results are very encouraging, there is some concern over the level of accuracy of the drag levels computed by the PPW code (Ref. 11, p. 139) or that this accuracy might be significantly reduced at low aspect ratios or for nonplanar configurations. For example, there is no complete treatment of the three-dimensional boundary layers that form in the wing/winglet and wing/body junctures. Also, the flowfields on the body and on the winglets are not interacted with any viscous boundary-layer calculation. To date, no complete assessment of these concerns has been made. However, it is noted that the predicted pressure drag reductions (Table 2) are in all instances somewhat less than the maximum achievable reduction in induced drag as predicted by the far-field drag model.

Some insight into accuracy of the PPW code calculated drag has been obtained in Ref. 30 by plotting the calculated PPW pressure drag coefficient in drag counts vs Mach number for an uncambered, untwisted wing as shown in Fig. 11. For these results, the wing has a taper ratio of 0.2, aspect ratio of 2.5, wing leading-edge sweep of 44 deg, and NACA 64A006 thickness distribution. Calculated pressure drag is essentially zero (less than one count) for the wing-alone for $0.1 \leq M \leq 0.9$. Above $M = 0.9$, there is a very steep increase in C_{Dp}, indicating the onset of drag rise. Also shown in Fig. 11 are similar pressure drag results for the same wing with a short winglet [$\ell = 0.15(b/2)$, $\Lambda = 45$ deg]. Here, due to interference effects, the wing tip and winglet root incidences had to be reduced by trial and error until a wing-plus-winglet lift coefficient of zero was obtained. For these slightly twisted, uncambered wing/winglet geometries, the calculated pressure drag is essentially identical to that of the wing alone at $C_L = 0$. Thus, there is no evidence of any difference in the accuracy of the PPW drag coefficient calculation by pressure integration for the wing/winglet or wing-alone configurations, at least for these thickness dominated flows.

Conclusions

A preliminary numerical design study has been performed to assess the potential for drag reduction at a transonic cruise design point for winglets installed on low-aspect-ratio wings. All initial design geometries have been generated using linearized potential flow theory. These geometries have been modified as required to overcome linear flow limitations and then the performance has been analyzed using the PPW numerical nonlinear potential flow model. It has been found that the linear theory designs yield realistic converged flow predictions using the nonlinear analysis code at $M = 0.8$, $C_L \cong 0.3$ for wings of aspect ratios of 1.75-2.67 and leading-edge sweep angles of 45-60 deg. Realistic converged flow solutions were also obtained from the nonlinear analysis code for wing/winglet designs generated for a 50 deg leading-edge sweep winglet of length equal to 15% of the wing semispan, installed on the higher-aspect-ratio wing planforms. Here, converged transonic flow solutions were obtained only when winglet root toe-out and wing tip incidence were systematically altered to reduce the winglet and wing tip loading levels relative to those required by the linear theory design methods.

For the $0.15(b/2)$, 50 deg leading-edge sweep winglets, the predicted pressure drag coefficient reductions at the design point were about 15%, while total drag coefficient reductions were about 12% relative to the wing-alone design at the same lift. These predicted percentage reductions were largely independent of the basic wing aspect ratio and wing leading-edge sweep. For the $0.25(b/2)$, 45 deg leading-edge sweep winglet, a pressure drag coefficient reduction of 19% and a total drag coefficient reduction of 15% were predicted. Thus, it has been concluded that, at least for winglet lengths below 25% of the wing semispan, the fractional pressure drag reduction due to a winglet approaches the induced drag reduction predicted by a simple far-field induced drag model. This drag model predicts the fractional induced drag coefficient reduction, $1\text{-}1/k$, is simply related to the ratio of winglet length to wing semispan, in that $k \cong 1 + \ell/(b/2)$.

Thus, the simple basic premise that motivated the present study appears to be valid. Winglets appear to have the potential to achieve significantly larger drag force reductions when applied to low-aspect-ratio wings rather than ones with higher aspect ratios. This is because the percentage drag coefficient reduction at equal lift is relatively independent of wing aspect ratio, while the lift-to-drag ratio decreases with decreasing aspect ratio. Thus, the lower-aspect-ratio configuration develops a much larger drag force at equal lift and wing loading.

Acknowledgments

The work has been supported by NASA Langley Research Center under Grant NAG-1-625, Dr. James M. Luckring, technical monitor. NASA has also provided access to the Langley computer facility via TELENET, as well as the required computer run time. Several discussions with Charlie Boppe at Grumman and Ed Waggoner and Pam Phillips at NASA Langley were extremely helpful in learning to utilize the PPW code. Early discussions with Leroy Spearman at NASA Langley helped to clarify the basic concept. Finally, thanks are also due to Dr. Richard W. Barnwell at Langley for intitially suggesting this problem to the first author.

References

[1]Whitcomb, R. T., "A Design Approach and Selected Wind-Tunnel Results at High Subsonic Speeds for Wing-Tip Mounted Winglets," NASA TN D-8260, July 1976.

[2]Flechner, S. G., Jacobs, P. F., and Whitcomb, R. T., "A High Subsonic Speed Wind-Tunnel Investigation of Winglets on a Representative Second-Generation Jet Transport Wing," NASA TN D-8264, July 1976.

[3]Asai, K., "Theoretical Considerations in the Aerodynamic Effectiveness of Winglets," *Journal of Aircraft*, Vol. 22, July 1985, pp. 635-637.

[4]Reynolds, P. T., Gertsen, W. M., and Voorhess, C. G., "Gates Learjet Model 28/29, the First 'Longhorn' Learjet," AIAA Paper 78-1445, Aug. 1978.

[5]Cary, M. D., "A Parametric Analysis of Winglet Effects," M. S. Thesis, Air Force Institute of Technology, Wright-Patterson AFB, OH, Dec. 1976.

[6]Heyson, H. H., Riebe, G. D., and Fulton, C. L., "Theoretical Parametric Study of the Relative Advantages of Winglets and Wing-Tip Extensions,"NASA TP 1020, 1977.

[7]Gingrich, P. B., Child, R. D., and Panageas, G. N., "Aerodynamic Configuration Development of the Highly Maneuverable Aircraft Technology Remotely Piloted Research Vehicle," NASA CR-143841, June 1977.

[8]Laiosa, J., "Prediction of HiMAT RPRV Component Interference Effects at Transonic Speeds," AIAA Paper 85-0213, Jan. 1980.

[9]Boppe, C. W., and Stern, M. A., "Simulated Transonic Flows for

Aircraft with Nacelles, Pylons, and Winglets," AIAA Paper 80-0130, Jan. 1980.

[10]Boppe, C. W., "Transonic Flow Field Analysis for Wing-Fuselage Configurations," NASA CR-3243, May 1980.

[11]Boppe, C. W., "Aerodynamic Analysis for Aircraft with Nacelles, Pylons, and Winglets at Transonic Speeds," NASA CR-4066, April 1987.

[12]Hackett, J. E., "Vortex Drag and Its Reduction," AGARD-R-723, May 1985, Paper 8.

[13]Kuhlman, J. M., "Higher Order Farfield Drag Minimization for a Subcritical Wing Design Code," *Journal of Aircraft*, Vol. 17, Sept. 1980, pp. 648-655.

[14]Kuhlman, J. M. and Shu, J. -Y., "Computer Program Documentation for a Subcritical Wing Design Code Using Higher Order Farfield Drag Minimization," NASA CR-3457, Sept. 1981.

[15]Kuhlman, J. M., "Iterative Optimal Subcritical Aerodynamic Design Code Including Profile Drag," AIAA Paper 83-0012, Jan. 1983.

[16]Kuhlman, J. M., "Iterative Subcritical Wing-Design Program for Minimum Total Drag," NASA Technical Progress Report, Grant NSG-1357, Nov. 1981

[17]Kuhlman, J. M., "Numerical Optimization Techniques for Bound Circulation Distribution for Minimum Induced Drag of Nonplanar Wings: Basic Formulations," NASA CR-3154, June 1979.

[18]Lundry, J. L. and Lissaman, P. B. S., "A Numerical Solution for the Minimum Induced Drag of Nonplanar Wings," *Journal of Aircraft*, Vol. 5, Jan.-Feb. 1968, pp. 17-21.

[19]*Janes' All the Worlds Aircraft, 1984-85—75th Anniversary Issue*, Janes' Publishing Co., London, 1985.

[20]Mann, M. J., Campbell, R. L., and Ferris, J. C., "Aerodynamic Design for Improved Maneuvarability by Use of Three-Dimensional Transonic Theory," NASA TP 2282, Feb. 1984.

[21]Bhateley, I. C., Mann, M. J., and Ballhaus, W. F., "Evaluation of Three-Dimensional Transonic Methods for the Analysis of Fighter Configurations," AIAA Paper 79-1528, July 1979.

[22]"Special Report: Advanced Fighter Technology," *Aviation Week and Space Technology*, June 1986, pp. 48-176.

[23]Vincent, J., "New Technologies for a European Fighter," *Aerospace America*, Vol. 24, June 1986, pp. 34-36.

[24]Langereux, P., "Rafale Will Keep Tricolor Flying," *Aerospace America*, Vol. 24, June 1986, pp. 26-30.

[25]Erickson, G. E. and Rogers, L. W., "Experimental Investigation at Low- and High-Subsonic Speeds of a Moderately Swept Fighter Wing with Deflected Leading-Edge Flaps," *Vortex Flow Aerodynamics Conference*, NASA CP-2417, Oct. 1985, pp. 141-168.

[26]Waggoner, E. G., "Computational Transonic Analysis for a Supercritical Transport Wing-Body Configuration," AIAA Paper 80-0129, Jan. 1980.

[27]Kuhlman, J. M., Liaw, P., and Cerney, M. J., "Theoretical/Numerical Study of Feasibility of Use of Winglets on Low Aspect Ratio Wings at Subsonic and Transonic Mach Numbers to Reduce Drag," NASA CR-4174, Aug. 1988.

[28]Bradley, R. G. and Bhateley, I. C., "Computational Aerodynamic Design of Fighter Aircraft-Progress and Pitfalls," AIAA Paper 83-2063, Aug. 1983.

[29]Hall, J. F., Neuhart, D. H., and Walkley, K. B., "An Interactive Graphics Program for Manipulation and Display of Panel Method Geometry," NASA CR-166098, March 1983.

[30]Kuhlman, J. M., Cerney, M. J., and Liaw, P., "Transonic Low Aspect Ratio Wing-Winglet Designs," AIAA Paper 88-0007, Jan. 1988.